

Influence of rockmass property variations on pre-mining stresses: a case study

Shahé Shnorhokian & Hani Mitri

McGill University, Montréal, Québec, Canada

Lindsay Moreau-Verlaan

Vale Canada Limited, Ontario Operations, Sudbury, Ontario, Canada



Challenges from North to South

Des défis du Nord au Sud

ABSTRACT

Variations in rockmass properties are commonly encountered in underground mines. When undertaking numerical modeling, the selection of different rockmass input properties can result in a wide range of results. In this paper, a simplified mine-wide model of a deep Canadian metal mine is constructed in FLAC^{3D} to study the influence of variations in rockmass properties on pre-mining stresses at two drift locations 1500 m below ground surface. It is calibrated using boundary tractions based on an in-situ stress measurement point. Laboratory results and borehole data are analyzed to determine the minimum, average, most likely, and maximum rockmass strength levels. It is observed that pre-mining stresses plotted for the drift locations follow regular patterns that depend on the rockmass properties of the formation in which the readings are taken, as well as other influential units. The methodology uses a range of vertical stress values to narrow down a large number of variations in rockmass properties into a smaller set that is realistically possible in the field. It is shown that the possible range of stress levels at locations of interest can be assessed, and key formations that influence the readings identified.

RÉSUMÉ

Des variations dans les propriétés des roches sont très communes dans les mines souterraines. Quand ces propriétés sont requises pour la modélisation numérique, des résultats très différents peuvent être obtenus. Dans le cadre de cette étude, un modèle conceptuel d'une mine profonde au Canada est élaboré dans FLAC^{3D} afin d'étudier l'influence de la variabilité des propriétés de la roche sur l'état des contraintes avant l'ouverture de la mine pour deux galeries situées à 1500 m de profondeur. Une pression est appliquée aux extrémités du modèle et celui-ci est calibré à l'aide de mesures de contraintes in situ. Les essais de laboratoire et les données de forage sont analysés afin d'obtenir les résistances minimales, moyennes, les plus probables, et maximales. Nous observons que les contraintes en pré-mine déterminées à l'emplacement des galeries suivent des tendances régulières qui dépendent des propriétés de la formation dans laquelle les observations sont effectuées et des propriétés d'autres unités. L'approche décrite utilise une plage réduite de valeurs de σ_{zz} afin de restreindre la variabilité des propriétés du massif de roche en un ensemble plausible à l'échelle du site. Nous montrons par ailleurs que la plage des états de contrainte possibles peut être évaluée à différents endroits, et que les formations influençant le plus les mesures peuvent être identifiées.

1 INTRODUCTION

Rocks are unique in terms of material properties in that their characteristics cannot be designed by an engineer, nor can they be manufactured with respect to certain guidelines. Rather, it is the engineer who needs to use ingenuity to adjust designs and procedures based on rock properties. In geotechnical work, rock is encountered at depths below the overburden profile but in underground mining, it is the sole material that encompasses the work environment from all sides. A realistic assessment of rock properties and their variations in the field is therefore crucial in any mining engineering design task.

Due to their genesis, geological history, and mineral composition, rocks vary greatly in terms of engineering properties. The unconfined compressive strength (UCS) of granite in South Africa can be somewhat different than in the Canadian Shield, for example, even if both values are within the same range. Adding to the complexity of the issue is the difference between intact rock and rockmass properties. In the example above, the same granite at two locations at a mine site in the Canadian Shield may give

identical UCS results in the laboratory but have different rockmass properties at various locations based on their Rock Mass Rating (RMR) value. This can be due to heavy jointing within a shear zone at one of the locations, while the rockmass elsewhere may still be in massive form.

During past decades, researchers have used different approaches – be they analytical, empirical, and statistical, amongst others – to predict rockmass properties due to variations in laboratory and field data. Numerical modeling is a relatively recent technique that has nevertheless become an integral part of the mining industry. Modeling can be used in the analysis of mining-induced stresses, microseismicity, and stope sequence scenarios, and a comprehensive review of its use in rock mechanics has been conducted by Jing (2003). When it is used for examining the impact of differences in rockmass properties, modeling is usually conducted in the form of a parametric study. Souley et al. (1997) studied the effect of constitutive laws for joints on displacements near an underground tunnel. Bhasin and Høeg (1998a, 1998b) examined the effects of block size and joint characteristics on shear strength and deformational properties. Cai

(2008) used variations in the Young's Modulus to generate a heterogeneous rockmass model to examine the influence of the intermediate principal stress on rock strength and fracturing. Edelbro (2010) examined the effect of changes in cohesion and internal angle of friction on stresses, factors of safety, and yielded zones in a tunnel and an ore raise in Scandinavia. Snelling et al. (2013) and Mercer and Bawden (2005a; 2005b) conducted parametric and statistical analyses with respect to microseismicity at the Creighton Mine in Sudbury.

In this paper, variations in rockmass properties at an underground Canadian metal mine are studied with a mine-wide numerical model constructed in FLAC^{3D}, and using data from laboratory tests and borehole logs. The impact of changes in the strength level of geological units, both individually and as groups of formations, is assessed with respect to the pre-mining stress read at the locations of two drifts on Level 4900 (1494 m).

2 METHODOLOGY

Vale's Garson Mine is located in the southeast section of the Sudbury Basin and has been in operation for more than 100 years. Two primary orebodies, designated as #1 Shear and #4 Shear, are located between 1200 and 1700 m below surface and dip 60-75° to the south. The sheared host rocks, which are collectively called the greenstone formation, include norites to the north and metasediments to the south. An olivine diabase dyke runs through the mine in a NW-SE direction with an average thickness of 30 m. It branches into a northern section (north dyke) that runs parallel to and above #4 Shear orebody in a W-E trend, and a southern section (south dyke), which runs NW-SE and bisects the orebodies into western and eastern segments – #1 Shear West, #1 Shear East, #4 Shear West, and #4 Shear East. Structural features include a shear zone 15 m in width, running NW-SE almost parallel and close to the south dyke.

2.1 Mine-wide numerical model

A mine-wide numerical model was constructed in FLAC^{3D} comprising the six major geological formations; norite, north/south dyke, interdyke norite, orebodies, greenstone, and metasediments. The dimensions of the model were 3000 ft (914 m) in the E-W direction, 2500 ft (762 m) in the N-S direction, and extending from Levels 5500 (1676 m) to 3500 (1067 m). It was calibrated using the boundary traction method – applying stresses only to the model boundaries – as first suggested by McKinnon (2001) and further developed for models having a heterogeneous rockmass (Shnorhokian et al. 2014). An in-situ stress measurement point on Level 4900 (1494 m) reported by Maloney and Cai (2006) was used as the main point of comparison to model readings for calibration purposes. The model comprised 1.15 million zones and required 8-10 hours to reach equilibrium and provide the pre-mining stresses.

Since the objective of this study was to examine the effect of variations in rockmass properties, the main

model was deemed to be digitally inefficient due to its large size and long time needed to attain equilibrium when considering the numerous changes required in input parameters. Hence, a simplified model was constructed in which all the geological formations were present but followed the overall shape and directions of their field counterparts, rather than being exact replicas as the main model. The simplified model comprised 585000 zones and needed three hours to reach equilibrium, making it an ideal choice for studying a large number of combinations examining variations in rockmass properties. It was also calibrated using boundary tractions and the in-situ stress measurement point on Level 4900. The formations and the calibration point are shown on this level in Figure 1.

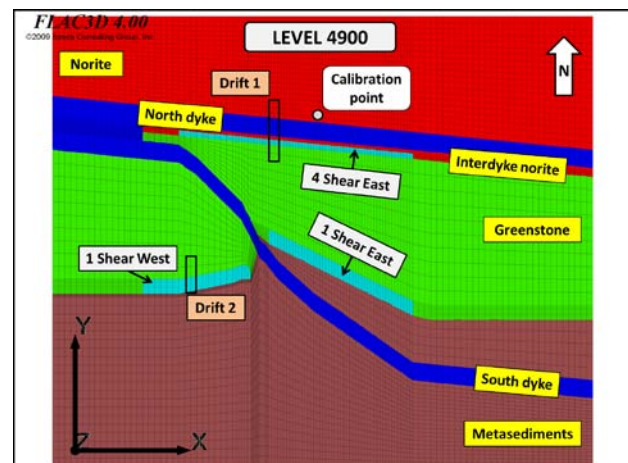


Figure 1. Geological formations, calibration point, and location of the two drifts on Level 4900 (plan view)

2.2 Rock and rockmass properties

Suorineni and Grasselli (2005) conducted laboratory tests on 44 samples taken from all formations present at the mine, which were combined with RMR data from borehole logs to derive the rockmass properties of the geological units. The software RocLab was used for this purpose to obtain the rockmass Young's (E_{rm}), bulk (K), and shear (G) moduli. The average RMR and range of mechanical properties, as well as RMR values from the borehole logs, are presented in Table 1.

Table 1. Laboratory test results and RMR values of units

Geological formation	Density (kg/m ³)	E_{intact} (MPa)	Poisson's Ratio ν	UCS (MPa)	RMR
Greenstone	2989	43-187	0.14-0.45	36-345	42-83
Dyke	3001	62-162	0.17-0.32	59-315	52-66
Meta-sediments	2768	34-91	0.16-0.32	77-185	32-75
Norite	2919	71-178	0.20-0.28	68-201	50-76
Interdyke norite	2893	147-178	0.21-0.27	181-201	45-68
Orebodies	4531	56-72	0.30-0.43	73-91	70-80

As can be observed, the results show a wide range of variation for most of the formations. For example, the UCS values for the dyke vary between 59 and 315 MPa for the nine samples tested from this geological unit. In addition, the greenstone formation is composed of three sub-units; amphibolites, metabasalts, and greenstones, each of which has its own range of variations. Apart from the laboratory results, RMR values sometimes show considerable variations as in the range between 32 and 75 for the metasediments.

Since rockmass properties are derived from these two sources (laboratory results and RMR values), it is vital to understand the combined effect of their variations on results. This is especially critical in numerical analysis as rockmass properties are used for model input parameters, and appreciable differences amongst them translate into wide variations in the results. In order to assess their full impact, the laboratory test results for each geological formation were first analyzed based on the UCS and Young's Modulus (E_i) values over their entire range, with different intervals evaluated in terms of the number of samples they comprised. Based on this analysis, only samples falling into the highest frequency intervals were retained to ensure the values used were representative, which reduced their total number from 44 to 27. Similarly, the RMR values for each formation were analyzed and minimum, average, and maximum categories determined.

Each of the 27 retained samples was then combined with the minimum, average, and maximum RMR for its formation to derive its E_{rm} and other parameters. Hence, from the 27 filtered samples, 81 rockmass properties were obtained for the six geological formations. Based on this dataset, minimum (softest), average, and maximum (stiffest) rockmass properties were determined for each geological formation based on its E_{rm} , which provides information regarding the stiffness of a geological unit. Since E_{rm} is related to the strength of the rockmass as well, the terms "weak" and "strong" are used in this study to be more perceptive. A fourth category, designated as most likely, was derived by combining a sample result from the highest frequency interval with the most frequent RMR value for that formation. Table 2 presents the weak, average, most likely, and strong values used as model input parameters for the different formations.

Table 2. E_{rm} (MPa) of all formations: weak, average, most likely, and strong

Geological formation	Weak	Average	Most likely	Strong	% model volume
Greenstone	8358	34654	51914	126856	28.42
Dyke	9552	53471	72167	127214	8.67
Meta-sediments	3582	23038	19140	66855	35.15
Norite	44611	95739	54019	143980	24.60
Interdyke norite	11266	28401	23723	55836	1.15
Oreboodies	35250	45484	52763	58777	2.01

2.3 Vertical stress (σ_{zz}) traction

At depth, the vertical stress (σ_{zz}) is due to the weight of overlying rock (Brown and Hoek 1978), and is usually taken to coincide with the minor principal stress (σ_3). When using the boundary traction approach in numerical analysis, the horizontal tractions required for calibration are observed to be much lower than the actual tectonic stresses at that depth (McKinnon 2001, Shnorhokian et al. 2014). The vertical traction, on the other hand, is usually close to the actual σ_{zz} value at that depth. Since it is based on the density of the overlying rock (ρ), gravity (g), and depth (H), σ_{zz} can be calculated using Equation 1 (Jaeger et al. 2007):

$$\sigma_{zz} = \rho * g * H \quad [1]$$

This characteristic of σ_{zz} allows its use as a filter to assess which combinations of rockmass properties are realistically possible in the field. Numerical models with various combinations of properties can be calibrated with respect to the measurement point on Level 4900 (1494 m), but the theoretical σ_{zz} traction needed for calibration, calculated based on the density of overlying rocks, can be used as an indicator of whether a particular combination is realistic.

Geological maps of the Garson Mine area indicate that the formations present at the model depth outcrop at the ground surface, with the exception of the orebodies that extend upwards to 1200 m below surface. Therefore, the densities of the different geological formations can be used to calculate the theoretical σ_{zz} acting at the top of the model at Level 3500 (1067 m). Based on the average density values from Table 1, and the relative volume of each formation in the model from Table 2, the weighted density of the simplified model was calculated to be 2925 kg/m³. For a depth of 1067 m, this translates to a vertical traction of 30.60 MPa, and allowing for a 10% variation on either side, the realistic σ_{zz} envelope would therefore range from 27.54 to 33.67 MPa. Even though the orebodies do not reach the surface and have the highest densities, their presence or absence does not make a significant difference in the σ_{zz} calculated due to their relatively small volume (2.01%) in the model. Hence, all combinations of rockmass properties in this study were assessed based on this interval and those that required σ_{zz} tractions outside of it were deemed to be unrealistic.

2.4 Variations in rockmass properties

To limit the total number of combinations of rockmass properties, the geological formations were divided into two categories. The norite and metasediments were termed as border units since they were located at the northern and southern ends of the model. As the mining activities were concentrated in the central regions, the north/south dyke, interdyke norite, greenstone, and orebodies were designated as core formations, and most of the variations studied in this paper centred on them. In the first phase, all core formations were kept at the same strength levels

while those of boundary formations varied between the four levels indicated in Table 2. This resulted in a total of 16 combinations calibrated individually at this stage. In the second phase, border formations were kept at their most likely strength levels and the four core formations were individually assigned their respective weak and strong values, while the other three were kept at their respective weak, average, most likely, and strong levels. In addition, the formation with the highest impact on the results was also examined in terms of its average and most likely levels, producing 30 combinations in total at this stage, each of which was calibrated separately.

2.5 Locations of N-S drifts

In order to examine the impact of different combinations of rockmass properties on the numerical results, the locations of two drifts running north-south were monitored in terms of pre-mining stresses. The first extended from the norite formation across the north dyke, interdyke norite, #4 Shear East, and reached the greenstone unit in the south on Level 4900 (1494 m), thus connecting the drifts and crosscuts serving that orebody and those of #1 Shear East. The second drift was located near #1 Shear West on the same level and reached into the orebody from the adjacent greenstone unit in the form of a crosscut access. The locations of the two drifts are indicated in Figure 1 and points were selected within each formation along their lengths at which pre-mining stresses were monitored. The first drift comprised a total of five monitoring points, with one in each of the norite, north dyke, interdyke norite, orebody, and greenstone units, while the second one included a monitoring point in each of the greenstone and orebody units.

3 RESULTS AND DISCUSSION

3.1 Phase 1: variations in border and core formations

The first phase of the study comprised changing the properties of all core formations between the four strength levels while keeping the boundary ones constant at their respective weak, average, most likely, and strong levels.

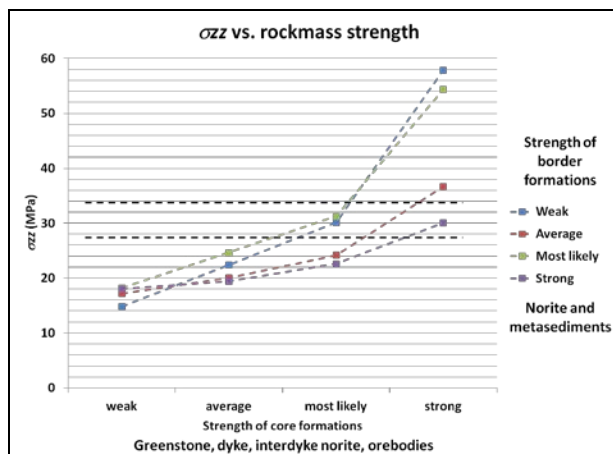


Figure 2. E_m (border and core formations) vs. σ_{zz}

The σ_{zz} traction required for the calibration of these 16 models is plotted in Figure 2 against the strength levels of core formations for different border conditions. Each border condition plot is designated a principal curve against which variations in properties of core formations can be assessed. In addition, the upper and lower limits of the theoretical σ_{zz} value are plotted and form an envelope within which all realistic combinations of rockmass properties should fall.

Several assessments can be made based on these results. Firstly, it is observed that regardless of strength level of the border formations, the σ_{zz} is lowest when all core formations are at their weak levels, and highest when they are all at their maximum strength. This means that for a given strength level of border formations, σ_{zz} cannot be lower than when all core formations are at their weakest and cannot be higher than when they are at their strongest. Secondly, the difference between the lowest and highest σ_{zz} values for a principal curve is largest when the border formations are at their weak (43 MPa difference) and most likely (36.15 MPa) strength levels, and smallest when they are at their average (19.42 MPa) and strong (12.04 MPa) levels. This implies that when the border formations are at their strongest, even the largest possible difference in σ_{zz} values may not be as significant as expected. Based on this, it can be concluded that the strength level of the two border formations has a very significant impact on the σ_{zz} required for calibration. This is not surprising because in terms of relative volume, the norite and metasediments comprise 24.60 and 35.15%, respectively, of the simplified model, which is about 60% combined.

In terms of the σ_{zz} envelope, the usefulness of Figure 2 is that it evaluates which of these 16 combinations are realistically possible. Since the densities of the different formations are known, and a 10% change on either side of 30.60 MPa was calculated to allow for local variations, it can be observed that only three of the 16 combinations are realistically possible in the field. Furthermore, the results validate the filtering process conducted on the laboratory test results and RMR values in that the combination of most likely strength levels for both border and core formations plots within the envelope at 31.24 MPa, and varies only 2.09% from the ideal 30.60 MPa calculated based on the weighted densities. Figure 2 indicates the usefulness of the σ_{zz} approach in examining numerous potential combinations of rockmass properties. Instead of conducting a simple parametric study, multiple combinations of strength levels for each formation can be evaluated as to whether they are realistically possible in the field based on the σ_{zz} required for calibration.

3.2 Phase 2: variations in individual core formations

In Phase 2 of this study, a single border strength level was chosen as a basis for analyzing the individual impact of core formations so as to minimize the total number of potential combinations. The most likely condition for the border formations was chosen for several reasons. Firstly, due to the relative frequency of laboratory tests and RMR values, this was the condition under which the norite and metasediments had the highest probability of being found.

Secondly, in addition to the weak border formation principal curve, the most likely one indicated the largest difference in σ_{zz} between its weak and strong core strength levels. This meant that any variations due to individual strength levels would be significant enough to be noted, which would not be the case for the strong border formation principal curve, for example. The latter had the smallest difference between the two extreme conditions of its core formations, and hence individual changes would have an even smaller impact on changes in σ_{zz} values.

With the border formations at their respective most likely levels, core formations – north/south dyke, interdyke norite, orebodies, and greenstone – were individually assigned their weak and strong rockmass properties in turn as the rest varied between their respective weak, average, most likely, and strong levels. This was done so as to maximize deviations from the principal curve and assess the impact of changes due to each core formation. The results of the additional 24 combinations are plotted in Figures 3 and 4, respectively, for the greenstone and the three other formations.

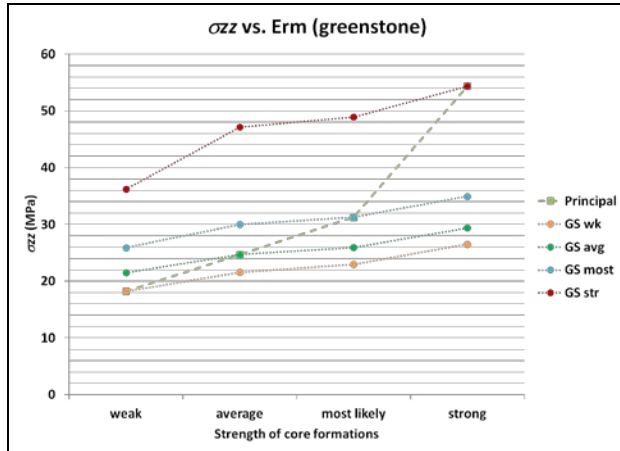


Figure 3. E_{rm} of greenstone formation vs. σ_{zz}

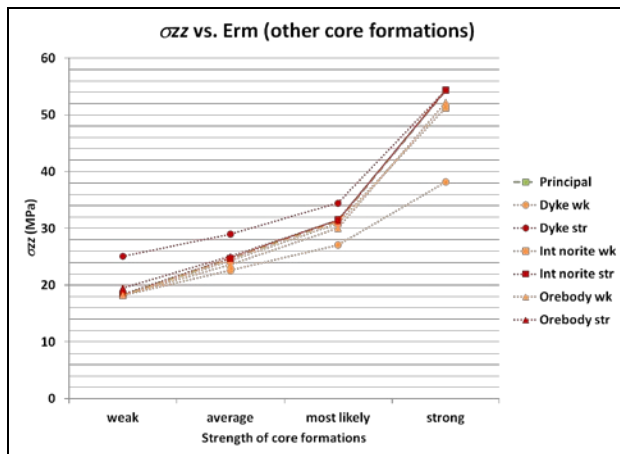


Figure 4. E_{rm} of other core formations vs. σ_{zz}

It can be observed in Figure 3 that the impact of the greenstone formation is the highest in terms of deviation

from the most likely principal curve. This is especially true for the two extreme ends where the greenstone formation is at its strongest while other core formations are at their weakest, and vice versa. A difference of 18 MPa in σ_{zz} is seen in the former and 28 MPa in the latter, and the high impact can be assigned once again to the relative volume of the greenstone formation. At 28.42%, it is the second most abundant geological unit, surpassing even the norite formation. The second in terms of impact on σ_{zz} is the dyke with maximum variations of 7 to 16 MPa from the most likely principal curve at either end (Figure 4). Once again, the impact is directly proportional to the relative volume of this formation, which stands at 8.67% when the north and south dykes are combined. The orebodies and interdyke norite are seen to have a minimal impact on the overall σ_{zz} value and their plots almost coincide with the principal curve. At 2.01% and 1.15%, respectively, of the total model volume, the link between relative abundance and individual impact is once again underlined.

When the σ_{zz} envelope is used to determine whether a certain combination of rockmass properties is realistically possible, all points on the weak and strong curves for the greenstone formation are eliminated as seen in Figure 3. Due to its high impact on the σ_{zz} traction, the six points plot outside the envelope of realistic values. In order to assess other possibilities, the average and most likely strength levels of this unit need to be considered as well, and this is done at the next stage. With respect to the dyke, only one point for its strong condition curve plots within the envelope and a point on its weak condition curve comes very close at 27.10 MPa as can be seen in Figure 4. While the two curves are separated enough from the principal one to indicate appreciable deviations, they are not far enough to warrant additional assessments regarding the average and most likely levels of the dyke. In terms of the orebodies and interdyke norite, their weak and strong curves almost coincide with the principal one and therefore the only points that fall within the envelope comprise the same conditions as the principal curve, which is when the rest of the core formations are at their most likely strength levels. A total of six points, counting the 27.10 MPa due to its proximity to the envelope, are observed to fall with the realistic σ_{zz} range.

As an additional evaluation of this phase of the study, the average and most likely levels of the greenstone were examined while varying the properties for the rest of the core formations, and the results of these additional six combinations are plotted in Figure 3 along with the former two curves discussed above. The average and most likely ones are observed to plot parallel to the weak and strong curves but are located closer to the former. However, only two points from the two additional curves – one from each of them – plot within the σ_{zz} envelope.

From a total of 31 combinations of variations in the properties of individual core formations based on the most likely principal curve, only eight fall within the realistic σ_{zz} envelope, with a ninth just outside it, and are considered as actual possibilities in the field. From a grand total of 46 models, the σ_{zz} envelope methodology limits the range of realistic possibilities to only 12. When the long periods of time for individual model calibration are considered, and

further analysis with respect to mining-induced stresses is contemplated, the ability to select only 25% of the original combinations due to their being realistic possibilities is an advantage. In addition to thus reducing the dataset, the methodology can also indicate the possible range of pre-mining stresses at points of interest.

3.3 Phase 2: variations in pre-mining stresses

In the previous sections, the results of the analysis of variations in rockmass properties in the border and core formations (combined and individual) were discussed with respect to the realistic σ_{zz} envelope. Pre-mining stresses are one of the main outputs of a calibrated numerical model and they are usually monitored at points of interest where important infrastructure or developments are being planned. In this study, the locations of two N-S drifts were used to examine the impact of variations in rockmass properties and to determine if the σ_{zz} envelope could be useful in providing a range of pre-mining stresses for planning and design purposes. As shown in Figure 1, the N-S drifts are located on Level 4900 (1494 m) and cut across the #4 Shear East and #1 Shear West orebodies. From an initial assessment of monitoring points along the two drifts, it was observed that the largest variations in pre-mining stresses occurred within the north dyke, orebody, and greenstone formations, while those in the norite and interdyke norite units were minimal.

Figure 5 plots the major principal stress (σ_1) at the monitoring point within the north dyke along the first drift for all nine combinations that fall within – or close to – the realistic σ_{zz} envelope (27.54 to 33.67 MPa) against the E_{rm} of the dyke. The points are plotted to indicate which formation's variations are responsible for that reading. As expected, it is observed that the stress increases linearly with increasing rockmass strength, with the minimum and maximum σ_1 levels expected at 54 MPa and 149 MPa, respectively, while most points plot at 94 MPa. This indicates that despite a difference of about 100 MPa between the two extremes, the most likely expected values is approximately midway in between. Hence, using the output from the calibrated models, the realistic pre-mining stresses for the different combinations can be read at locations of interest.

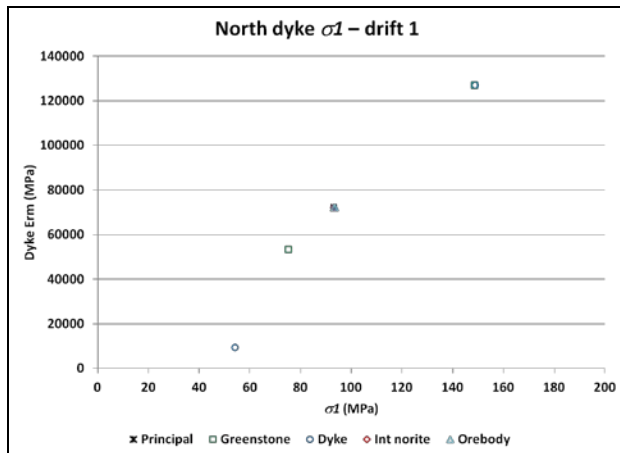


Figure 5. Drift 1 – north dyke: σ_1 vs. E_{rm}

Figure 6 plots σ_1 at the #4 Shear East monitoring point along the first drift for the same nine combinations and a similar pattern can be observed here, with some notable differences. Firstly, the range of possible stress values is somewhat narrower as it lies between 68 and 120 MPa, with most points plotting at around 111 MPa. Secondly, at the same E_{rm} value, the #4 Shear East monitoring point exhibits notable changes in σ_1 especially at its most likely strength level changes in the properties of the dyke take place. This means that while the stress level at this point depends mainly on the E_{rm} of #4 Shear East, it is also influenced by the north dyke, reducing σ_1 by 10 MPa.

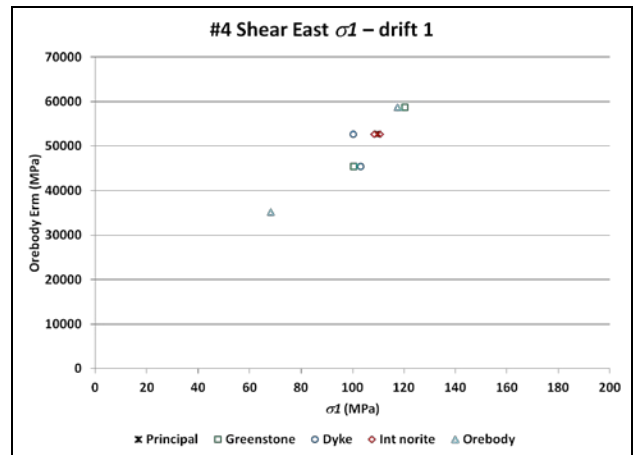


Figure 6. Drift 1 – #4 Shear East: σ_1 vs. E_{rm}

In Figure 7, the values at the monitoring point within the greenstone formation along the first drift are plotted, and the same pattern is observed. The most likely values congregate around 78 MPa but the overall range extends from 63 to 80 MPa. Despite its having the second largest relative volume, readings in the greenstone formation for the same strength level are also influenced by the north dyke as observed by one of its points plotting away from the main set. Figure 7 shows that when the former is at its most likely values, stress levels are reduced by 4-5 MPa when the dyke is at its weakest.

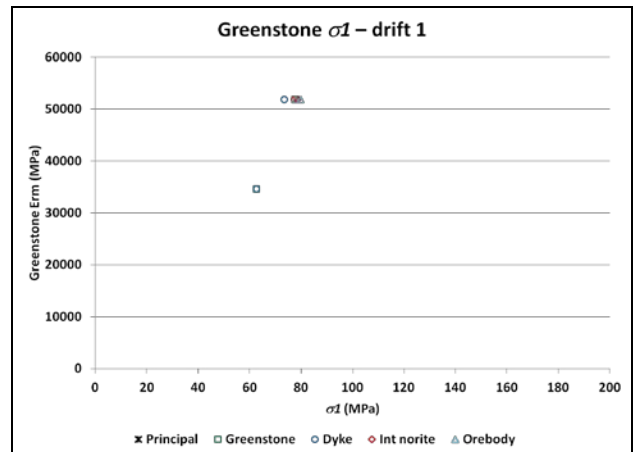


Figure 7. Drift 1 – greenstone: σ_1 vs. E_{rm}

Hence, when pre-mining stress levels along the first drift are evaluated, it is observed that the methodology is able to reduce the initial number of combinations to a realistic few, and to indicate whether stresses at a given monitoring point in a geological unit are also influenced by other adjacent formations.

In terms of the second drift near #1 Shear West, the two monitoring points are located within the greenstone and orebody units. This presents an opportunity to compare the stress patterns to the same formations in the first drift for any similarities.

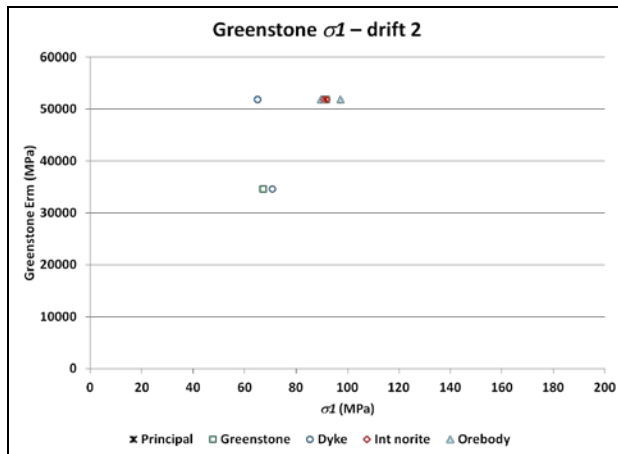


Figure 8. Drift 2 – greenstone: σ_1 vs. E_{rm}

Figure 8 presents the readings for the monitoring point within the greenstone formation and apart from the overall linear relationship between E_{rm} and σ_1 , it is observed that despite the same changes in strength levels, the values of the pre-mining major principal stress are limited within a narrower range than in the first drift. The minimum and maximum σ_1 read 65 and 97 MPa, respectively, with most of the points plotted at 90 MPa. However, in addition to the narrower range, it is interesting to note that changes in the dyke's properties has a high impact on the readings at this point to the extent of reducing them from 90 to 65 MPa.

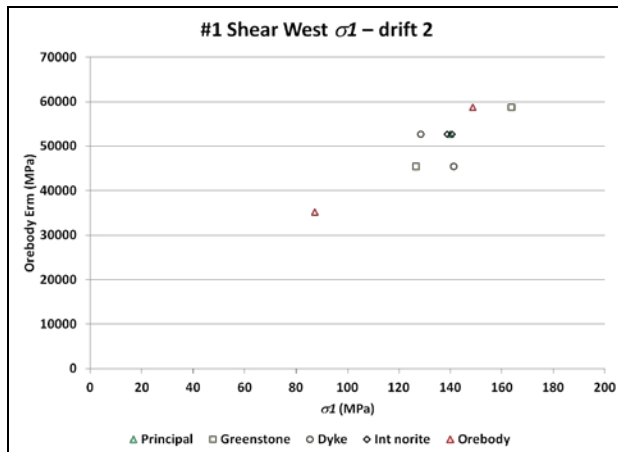


Figure 9. Drift 2 – #1 Shear West: σ_1 vs. E_{rm}

This is significant because it clearly indicates that readings in a given geological formation can vary greatly due to strength variations not only within that particular unit, but in the properties of an adjacent formation as well. Another advantage of the methodology is, therefore, that it provides an understanding of the influence of variations in other geological units on a given monitoring point.

Finally, Figure 9 plots the readings at the monitoring point within #1 Shear West, and a similar pattern to Figure 8 is noted. While the overall range from 87 to 164 MPa follows a linear pattern with respect to the orebody E_{rm} , most of the points congregate between 126 and 140 MPa. A dispersion of around 15 MPa is observed at a given E_{rm} at most strength levels. Based on the points plotting at some distance from the data groups, the greenstone and dyke are observed to be the formations responsible for this, which is not surprising bearing in mind that they are the most influential ones amongst the core units. While it was only the north dyke that influenced readings in #4 Shear East, the greenstone is observed to be influential as well in #1 Shear West.

4 CONCLUSIONS

A methodology was presented for conducting parametric studies with numerical modeling on variations in rockmass properties emanating from laboratory tests and borehole RMR data at Vale's Garson Mine. A simplified mine-wide model of the mine was constructed in FLAC^{3D} and strength properties assigned to the geological formations based on their respective weak, average, most likely, and strong levels. In the first stage, all four core units were kept at their same respective strength levels while those of the border formations were made to vary, and the resulting plots were designated as principal curves. It was noted that the largest variations occurred between the weak and strong levels of core formations within the weak and most likely principal curves. Using the range of σ_{zz} calculated from the densities of the formations present, only three of the 16 principal combinations were deemed as realistically possible. In the second phase, based on the most likely principal curve, the impact of individual variations was studied for each core formation using its respective weak and strong rockmass properties. Due to having the largest deviation from the principal curve in terms of σ_{zz} , average and most likely strength levels for the greenstone unit were also examined. The dyke was observed to have the second highest impact on σ_{zz} , while the interdyke norite and orebodies had minimal effects. In total, only nine out of the 31 combinations studied in this phase plotted within or very near to the realistic σ_{zz} envelope. In this phase, the major principal stress (σ_1) was monitored along two N-S drifts on Level 4900 (1494 m) cutting across #4 Shear East and #1 Shear West for these nine combinations. It was observed that while σ_1 varied linearly with the E_{rm} of the geological formation in which the monitoring point was located, the greenstone and dyke had significant impacts on readings as well, resulting in differences of up to 25 MPa. The methodology of using numerical analysis with a realistic σ_{zz} envelope

was seen to constitute an important tool in reducing a large number of combinations to a realistic set, to assess the minimum, most likely, and maximum stresses expected at locations of interest, and to identify the influential formations affecting readings at those points.

5 ACKNOWLEDGEMENTS

This work is financially supported by a research grant from the Natural Sciences and Engineering Research Council of Canada (NSERC) in partnership with Vale Canada Ltd through the Collaborative Research and Development (CRD) Program. The authors are grateful for their financial support.

6 REFERENCES

- Bhasin, R. and Hoeg, K. 1998a. Numerical modelling of block size effects and influence of joint properties in multiply jointed Rock. *Tunn. Under. Space Tech.*, 13(2): 181 – 188.
- Bhasin, R. and Hoeg, K. 1998b. Parametric study for a large cavern in jointed rock using a distinct element model (UDEC-BB). *Int. J. Rock Mech. Min. Sci.*, 35(1): 17 – 29.
- Brown, E.T. and Hoek, E. 1978. Trends in relationships between measured in-situ stresses and depth. *Intl. J. Rock Mech. Min. Sci. Geomech. Abstr.*, 15: 211 – 215.
- Cai, M. 2008. Influence of intermediate principal stress on rock fracturing and strength near excavation boundaries – insight from numerical modeling. *Int. J. Rock Mech. Min. Sci.*, 45: 763 – 772.
- Edelbro, C. 2010. Different approaches for simulating brittle failure in two hard rock mass cases: a parametric study. *Rock Mech. Rock Eng.*, 43: 151 – 165.
- Jaeger, J.C., Cook, N.G.W., and Zimmerman, R. 2007. *Fundamentals of rock mechanics*. 4th ed., Blackwell, Malden.
- Jing, L. 2003. A review of techniques, advances and outstanding issues in numerical modelling for rock mechanics and rock engineering. *Intl. J. Rock Mech. Min. Sci.*, 40: 283 – 353.
- Maloney, S. and Cai, M. 2006. *In situ stress determination – Garson Mine*. MIRARCO Project report 06-015.
- McKinnon, S.D. 2001. Analysis of stress measurements using a numerical model methodology. *Int. J. Rock Mech. Min. Sci.*, 38: 699 – 709.
- Mercer, R.A. and Bawden, W.F. 2005a. A statistical approach for the integrated analysis of mine induced seismicity and numerical stress estimates, a case study – Part I: developing the relations. *Intl. J. Rock Mech. Min. Sci.*, 42: 47 – 72.
- Mercer, R.A. and Bawden, W.F. 2005b. A statistical approach for the integrated analysis of mine induced seismicity and numerical stress estimates, a case study – Part II: evaluation of the relations. *Intl. J. Rock Mech. Min. Sci.*, 42: 73 – 94.
- Shnorhokian, S., Mitri, H.S., and Thibodeau, D., 2014. A methodology for calibrating numerical models with a heterogeneous rockmass. *Int. J. Rock Mech. Min. Sci.*, 70: 353 – 367.
- Snelling, P.E., Godin, L., and McKinnon, S.D. 2013. The role of geologic structure and stress in triggering remote seismicity in Creighton Mine, Sudbury, Canada. *Int. J. Rock Mech. Min. Sci.*, 58: 166 – 179.
- Souley, M., Hommand, F., and Thoraval, A. 1997. The effect of joint constitutive laws on the modelling of an underground excavation and comparison with in-situ measurements. *Intl. J. Rock Mech. Min. Sci.*, 34(1): 97 – 115.
- Suorineni, F.T. and Grasselli, G. 2005. *Rock strength tests – final report*. MIRARCO Mining Innovation. Sudbury.